Chemical Science

EDGE ARTICLE

View Article Online
View Journal | View Issue

Cite this: *Chem. Sci.*, 2016, 7, 6273

$[A_3X][Ga_3PS_8]$ (A = K, Rb; X = Cl, Br): promising IR non-linear optical materials exhibiting concurrently strong second-harmonic generation and high laser induced damage thresholds†

Bin-Wen Liu, Hui-Yi Zeng, Xiao-Ming Jiang, Guan-E Wang, Shu-Fang Li, Li Xu* and Guo-Cong Guo*

Received 1st May 2016
Accepted 1st June 2016

DOI: 10.1039/c6sc01907b

www.rsc.org/chemicalscience

Mid-far infrared (IR) non-linear optical (NLO) materials are of great importance in military and civil fields. However, commercial IR-NLO crystals (such as $AgGaS_2$, $AgGaSe_2$ and $ZnGeP_2$) do not currently satisfy the requirements of large second-harmonic generation (SHG) and high laser induced damage thresholds (LIDTs), which seriously limits their practical applications. Herein, we have developed a new series of salt-inclusion chalcogenides, $[A_3X][Ga_3PS_8]$ (A = K, Rb; X = Cl, Br), which are constructed from alternate stacking of adamantane-like $[Ga_3PS_{10}]^{6-}$ cluster layers and cationic $[A_3X]^{2+}$ salt layers. Importantly, they display both large SHG responses of several-fold and high LIDTs for dozens of times that of commercial $AgGaS_2$, which exhibit the highest LIDTs among the reported IR-NLO materials with a larger SHG conversion efficiency than that of $AgGaS_2$. These properties together with wide transparent region, type I phase-matching features and congruent-melting behaviors indicate they are promising IR-NLO materials.

Introduction

Second-order non-linear optical (NLO) materials are of current and broad interest in laser science and technology owing to their applications in producing new laser sources based on cascaded frequency conversion.[1] Many fundamental but rigorous rules are involved in selecting NLO materials for practical employment: (1) large second-order NLO susceptibility ($\chi^{(2)}$), (2) high laser induced damage thresholds (LIDTs), (3) suitable optical transparency, (4) phase-matching behavior, and (5) high-quality bulk single crystals. To date, many notable NLO crystals, such as KH_2PO_4 (KDP),[2] $KTiOPO_4$ (KTP),[3] β-BaB_2O_4 (BBO),[4] and LiB_3O_5 (LBO),[5] have been acquired. These oxide-based materials are favorably used in either the ultraviolet or visible region, but are generally restricted for application in the infrared (IR) region, owing to their short IR cut-off edge. In contrast, only a few IR-NLO materials, such as chalcopyrite semiconductors $AgGaS_2$ (AGS),[6] $AgGaSe_2$ (AGSe),[7] and $ZnGeP_2$ (ZGP),[8] are commercially used. They feature large NLO coefficients, but suffer from shortcomings of relatively low LIDTs, which is the main obstacle that limits their high-power laser applications. To overcome this problem, many works have been focused on designing new materials with wide band gaps,[9] which mainly include electropositive element-inclusion chalcogenides, such as $LiGaS_2$,[10] $LiInS_2$,[11] $Li_2Ga_2GeS_6$,[12] and $BaGa_4S_7$,[13] and metal halides such as $BaClBF_4$,[14] $NaSb_3F_{10}$,[15] and $Cs_2HgI_2Cl_2$.[16] These materials show improved LIDTs, however, they come at the expense of decreased NLO coefficients. For instance, the Li^+ substitution for Ag^+ in the AGS leads to the discovery of a new IR-NLO material, $LiGaS_2$, which possesses relatively higher LIDT that is afflicted with lower $\chi^{(2)}$ value of about half that of AGS. Such drawbacks make them insufficient for practical applications. Moreover, most of the other IR-NLO material systems are just at the stage of laboratory research. Consequently, exploration of new materials with both good NLO efficiency and LIDT is urgently needed in IR-NLO material science and laser technology.

Salt-inclusion compounds, an interesting class of host–guest materials, produce a mixed framework wherein species of different structures and functions can be assembled, which may lead to a new compounds possessing diverse structures, improved properties, and unique functions.[17] However, prior to our investigation, the salt-inclusion compounds reported were mainly oxides that are generally unfavorable to use as IR-NLO materials. Herein, we extend the exploration to salt-inclusion chalcogenides, resulting in the discovery of several novel IR-NLO material systems, $[K_3Cl][Ga_3PS_8]$ (**1**), $[Rb_3Cl][Ga_3PS_8]$ (**2**), $[K_3Br][Ga_3PS_8]$ (**3**), and $[Rb_3Br][Ga_3PS_8]$ (**4**), which were constructed from alternate stacking of adamantane-like $[Ga_3PS_{10}]^{6-}$ cluster layers and cationic $[A_3X]^{2+}$ (A = K, Rb; X = Cl, Br) layers

State Key Laboratory of Structural Chemistry, Fujian Institute of Research on the Structure of Matter, Chinese Academy of Sciences, Fuzhou 350002, P. R. China. E-mail: xli@fjirsm.ac.cn; gcguo@fjirsm.ac.cn

† Electronic supplementary information (ESI) available. CSD 429893–429896. For ESI and crystallographic data in CIF or other electronic format see DOI: 10.1039/c6sc01907b

along the *c*-axis. Remarkably, compounds **1–4** exhibit concurrently large SHG responses of 4, 5, 7, and 9 times at 1064 nm (1.0, 1.1, 1.2 and 2.0 times at 1950 nm) and high LIDTs of 39, 37, 32, and 31 times that of benchmark AGS, respectively. In addition, broad transparency range, type I phase-matching behaviors, as well as congruent-melting features indicate that they are promising IR-NLO materials.

Results and discussion

Colorless crystals of the title compounds were synthesized *via* a salt flux method with AX (A = K, Rb; X = Cl, Br) as the flux agents, in which the Cl-analogues (**1** and **2**) were isostructural and crystallize in the orthorhombic space group $Pmn2_1$, while the Br-analogues (**3** and **4**) were isostructural and are adopted in the monoclinic space group *Pm* (Table S1 in the ESI†). All of them feature a similar 2D structures formed by alternate stacking of adamantane-like $[Ga_3PS_{10}]^{6-}$ cluster layers and cationic $[A_3X]^{2+}$ layers, which exhibit hybrid frameworks with mixed covalent $[Ga_3PS_8]^{2-}$ and ionic $[A_3X]^{2+}$ salt sub-lattices (Fig. 1b and e).

In the structure of the Cl-analogues, three $[GaS_4]$ tetrahedra are corner-shared with each other to build a triangular tetrahedral trimer, on which the $[PS_4]$ tetrahedron is capping to yield an adamantane-like $[Ga_3PS_{10}]^{6-}$ cluster (Fig. 1a). Each $[Ga_3PS_{10}]^{6-}$ cluster shares two triangular corners S(4) along the *a*-direction to form a chain, which further shares the third triangular corner S(6) with the middle of triangular tetrahedral trimer in the neighboring chain along the *b*-direction to create an adamantane-like $[Ga_3PS_{10}]^{6-}$ cluster layer in the *ab*-plane (Fig. 1a), whereas the anionic layers in the Br-analogues have the same conformation as those in the Cl-analogues with the extending directions *a* and *b* exchanging (Fig. 1d). As listed in Table S2 and S3,† the Ga–S bond lengths and S–Ga–S bond angles in **1–4** are in the range of 2.225(1)–2.357(3) Å and 103.7(1)–115.1(1)°, respectively. These data are respectively comparable to those in related gallium sulfides, such as $PbGa_4S_7$,[18] $SnGa_4S_7$,[19] and $Ba_4CuGa_5S_{12}$.[20] The P–S bond distances and S–P–S bond angles in **1–4** fall in the range of 1.994(3)–2.112(4) Å and 105.7(1)–113.7(1)°, respectively, which are comparable to those in $AZrPS_6$ (A = K, Rb, Cs),[21] and $K_9Nd[PS_4]_4$.[22]

The cationic $[A_3X]^{2+}$ layers in **1–4** can be considered as constructed from the distorted X-centered quadrangular pyramids, $[XA_5]^{4+}$, which are corner-shared with each other along the *a*- and *b*-directions to become approximately co-planar with all the apexes pointing along the same direction, resulting in an acentric $[A_3X]^{2+}$ layer (Fig. 1c and f). The cationic $[A_3X]^{2+}$ and adamantane-like $[Ga_3PS_{10}]^{6-}$ cluster layers are further anchored to each other through A–S interactions (Fig. S3†) to build a pseudo 3D structure, in which the adjacent layers are highly acentric in nature stacked alternately along the *c*-axis and pack in a non-centrosymmetric (NCS) fashion.

Interestingly, despite having the same stoichiometric ratio and similar layer motif, the Cl-analogues and the Br-analogues crystallize in different space groups, which arises from the different stacking fashions of the anionic $[Ga_3PS_8]^{2-}$ layers and cationic $[A_3X]^{2+}$ layers along the *c*-axis. In the Br-analogues, the neighboring $[Ga_3PS_{10}]^{6-}$ cluster layers stack along the *c*-direction without a transversal shift in the *ab*-plane. Differently, the neighboring $[Ga_3PS_{10}]^{6-}$ cluster layers in the Cl-analogues are stacked with a shift of *a*/2 along the *a*-direction and a shift of 0.128*b* along the *b*-direction, which results in doubling the *c*-axis and unit cell volume. In comparison with Cl^- (ionic radius: 1.61 Å), the larger Br^- (ionic radius: 1.82 Å) anion in the X^- site make the $[A_3X]^{2+}$ salt sub-lattices different, which further leads to the interactions between the anionic and cationic layers changing, for example, the Rb(1)–S(1) interaction is weakened, as shown by their distances increasing from 3.700 Å in **2** to 4.024 Å in **4** (Fig. S3†). These variations originate from the $[A_3X]^{2+}$ salt sublattices changing and may be responsible for the change in the space group from $Pmn2_1$ for the Cl-analogues to *Pm* for the Br-analogues. Moreover, the acentric $[A_3X]^{2+}$ layer can greatly affect or directly determine the bulk acentricity, which demonstrates that the ionic salt in the salt-inclusion chalcogenide may act as a structure directing agent during the formation of the NCS compounds. These discoveries provide an enormous playground for further rational design of functional host–guest frameworks.

The differential scanning calorimetry (DSC) results show that compounds **1–4** undergoes melting upon heating and crystallization upon cooling events (Fig. 2). The powder XRD patterns of the residue from one melting/recrystallization cycle are in good agreement with those of the initially synthesized products and simulated ones from their CIFs (Fig. S4†), indicating these phases are congruently melting. When compared to the known IR-NLO materials, such as AGS (996 °C),[23] $LiGaS_2$ (1050 °C),[24] and $BaGa_4S_7$ (1090 °C),[13] compounds **1–4** have relatively lower melting temperatures (621, 655, 628 and 621 °C for **1–4**, respectively). These results reveal that large crystals for further physical property studies can be grown using the Bridgman method at lower temperatures.

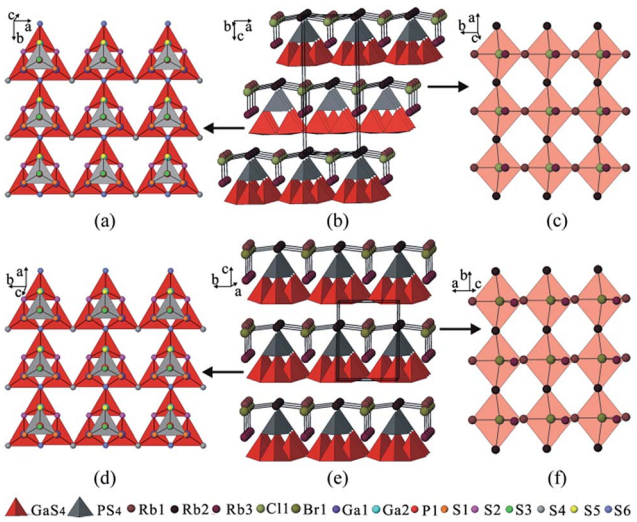

Fig. 1 The $[Ga_3PS_{10}]^{6-}$ cluster layers in **2** (a) and **4** (d), cationic $[A_3X]^{2+}$ layers in **2** (c) and **4** (f), and an overview of the 3D frameworks in **2** (b) and **4** (e). Compound **1** is isostructural to **2** and **3** is isostructural to **4**.

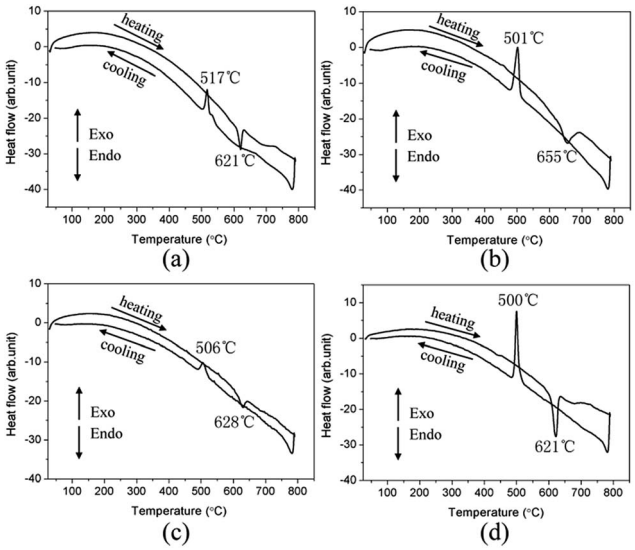

Fig. 2 DSC curves revealing the melting and recrystallization events of **1** (a), **2** (b), **3** (c) and **4** (d).

The UV-visible-NIR diffuse reflectance spectra in Fig. S5† shows strong absorption edges at 3.60, 3.65, 3.85, and 3.50 eV for **1–4**, respectively, which are comparable to those of Li-contained chalcogenides such as $LiGaS_2$ (3.87 eV),[10] $Li_2Ga_2GeS_6$ (3.65 eV),[12] and Li_2CdGeS_4 (3.15 eV).[25] In comparison with the values of AGS (2.62 eV)[26] and ZGP (1.75 eV),[8] compounds **1–4** have relatively wider band gaps, demonstrating that they can avoid two-photon absorption (TPA) of the conventional 1064 nm incident laser and subsequently benefit from an improved LIDT. The further absorption spectrum in Fig. S6† shows that the absorption peak at about 609 and 530 cm^{-1} was attributed to the intrinsic absorption of the P–S bond,[27] *i.e.*, there is no intrinsic absorption of chemical bonds in a broad spectral range from 0.35 to 16.5 μm (Fig. S5 and S6†), suggesting that they may be suitable for a variety of NLO applications in longer wavelength regions.

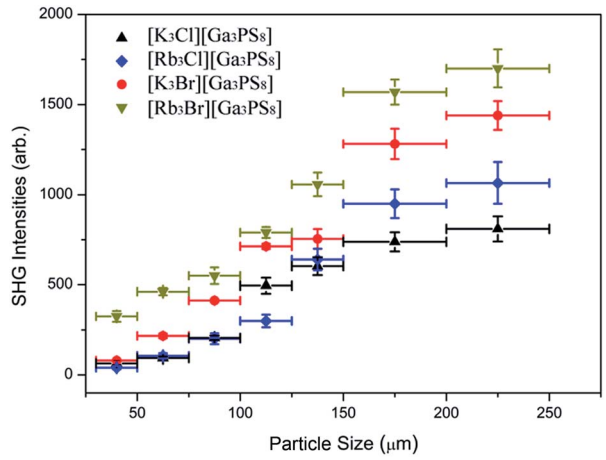

Fig. 3 The phase-matching results of **1–4**; the curve is to guide for the eye and is not a fit to the data. The particle size deviation and the SHG intensity deviation depending on the rotation angle are indicated by horizontal and vertical error bars, respectively.

Because $[GaS_4]$ and $[PS_4]$ tetrahedra are well known NLO-active building units and the cationic $[A_3X]^{2+}$ and adamantane-like $[Ga_3PS_{10}]^{6-}$ cluster layers are highly acentric in nature that pack in a NCS fashion, it can be expected that compounds **1–4** may achieve large SHG responses. Powder SHG measurements were carried out using a modified Kurtz powder method,[28] with a lower-intensity laser than the damage threshold of AGS. A polycrystalline AGS ($d_{eff} = 18$ pm V^{-1})[29] sample was used as the reference material. The SHG intensities of **1–4** increase upon increasing the particle size and then reach a relatively flat trend after a certain particle size using an incident laser at 1064 nm and 1950 nm (Fig. 3 and S7†), suggesting type I phase-matching behavior. Remarkably, compounds **1–4** possess large SHG signals of 4, 5, 7, and 9 times at 1064 nm (1.0, 1.1, 1.2 and 2.0 times at 1950 nm) that of AGS, respectively (Fig. S8†), in which the Br-analogues exhibited stronger SHG signals, followed by the Cl-analogues.

The powder LIDT data of **1–4** and benchmark AGS were accessed by the single pulse powder LIDT method.[30] As illustrated in Fig. 4 and Table S5,† the powder LIDTs of **1–4** are 78.5, 74.7, 64.5, and 61.2 MW cm^{-2} using an incident laser at 1064 nm, 10 ns and 1 Hz, showing 39, 37, 32, and 31 times that of AGS (2.0 MW cm^{-2}), respectively, which are larger than those of $Ba_4ZnGa_4Se_{10}Cl_2$ (17× AGS),[31] $Pb_{17}O_8Cl_{18}$ (12.8× AGS),[32] Cu_2ZnSiS_4 (~6× AGS),[33] $SnGa_4S_7$ (19× AGS),[19] Li_2CdGeS_4 (~17× AGS),[34] Na_2BaGeS_4 (8× AGS),[35] and $Na_2Hg_3Si_2S_8$ (4.5× AGS),[36] and are comparable to those of $Ba_8Sn_4S_{15}$ (26× AGS),[37] $Ba_2Ga_8GeS_{16}$ (22× AGS),[38] and Li_2MnGeS_4 (~40× AGS).[39] Importantly, it is worth noting that compounds **1–4** exhibit the highest LIDTs among the IR-NLO materials that have a larger SHG conversion efficiency than AGS. Their good thermal and chemical stability, as well as large band gaps, which can make these phases be able to sustain laser illumination at 1064 nm without invoking TPA problems, are believed to make a significant contribution to the improvement of LIDTs. These observations indicate that compounds **1–4** not only exhibit a strong SHG but also have high LIDTs, which should be good candidates for high-power IR-NLO applications.

To better understand the optical properties, theoretical calculations based on DFT methods were performed. The band structure calculations show that the Cl-analogues are indirect

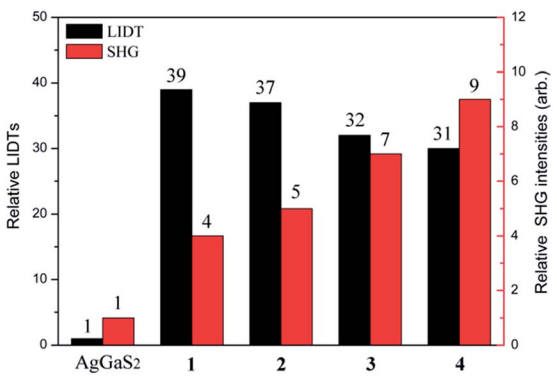

Fig. 4 The relative LIDTs and relative SHG intensities of **1–4** and AGS.

band structures with the band gaps of 2.26 and 2.36 eV for **1** and **2**, whereas the Br-analogues are direct band structures with band gaps of 2.60 and 2.48 eV for **3** and **4**, respectively (Fig. S9†). The bands can be assigned according to the total and partial DOSs in Fig. S10.† For **1–4**, the conductive bands (CBs) close to the Fermi level are mostly composed of Ga 4s and 4p, S 3p and P 3p states, mixing with small amounts of K 3p and 4s (Rb 4p and 5s) states, whereas the valence bands (VBs) close to the Fermi level originate predominately from S 3p and Cl 3p (Br 4p) states; therefore, their optical absorptions can mainly be ascribed to the charge transfer from the S 3p and Cl 3p (Br 4p) states to the Ga 4s and 4p, S 3p, P 3p and K 3p and 4s (Rb 4p and 5s) states.

To gain further insights into the NLO properties, calculations of the second-order NLO susceptibility were also performed to explain their SHG efficiencies. The calculated real part $\varepsilon_1(\omega)$ and the imaginary part $\varepsilon_2(\omega)$ of the frequency-dependent optical dielectric functions of **1–4** are illustrated in Fig. S11 and S12.† It can be found from the dispersion of the calculated $\varepsilon_2(\omega)$ spectra that the maximum absorption peaks are located at about 5.95 and 8.36 eV for **1**; 6.01 and 8.20 eV for **2**; 5.96 and 8.07 eV for **3**; and 5.57 and 7.65 eV for **4**, which are mainly attributed to the charge transfers from S 3p and Cl 3p (Br 4p) states to Ga 4s and 4p, S 3p, P 3p and K 3p and 4s (Rb 4p and 5s) states, according to the abovementioned DOS analysis. Under the restriction of Kleinman symmetry, the Cl- and Br-analogues have three and six independent second-order dielectric tensor elements due to their *mm*2 and *m* point symmetry, which are related to the SHG coefficients d_{15}, d_{24}, and d_{33}; as well as d_{11}, d_{12}, d_{13}, d_{15}, d_{24} and d_{33}, respectively. As shown in Fig. 5, the calculated d_{15}, d_{24} and d_{33} are 26.7, 26.1 and 26.5 pm V^{-1} for **1**, 30.7, 30.3, 29.8 pm V^{-1} for **2**; d_{11}, d_{12}, d_{13}, d_{15}, d_{24} and d_{33} coefficients are 45.2, 45.3, 44.1, 44.6, 45.0 and 43.6 pm V^{-1} for **3**, 50.9, 50.2, 49.2, 50.1, 49.7 and 48.5 pm V^{-1} for **4**, respectively, at the wavelength of 1064 nm (1.165 eV). This shows that the calculated average NLO coefficients d_{ij} display an increasing trend with the following order: **1** (22.5 pm V^{-1}) < **2** (25.6 pm V^{-1}) < **3** (44.6 pm V^{-1}) < **4** (49.7 pm V^{-1}), which is in accordance with the experimental observations.

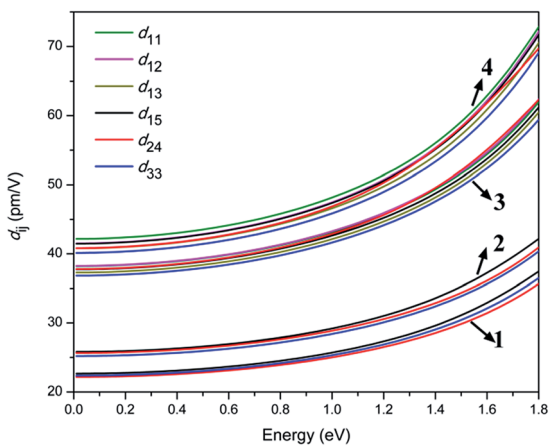

Fig. 5 The calculated frequency-dependent SHG coefficients of **1–4**.

Conclusions

In summary, a new series of salt-inclusion chalcogenides, $[A_3X][Ga_3PS_8]$ (A = K, Rb; X = Cl, Br), have been obtained using a salt flux method and display both large SHG responses of 4–9 times at 1064 nm (and 1–2 times at 1950 nm) and high LIDTs of 31–39 times that of the benchmark AGS, as well as a type I phase-matching feature. It is worth noting that these wide band gaps compounds exhibit the highest LIDTs among the IR-NLO materials that have a larger SHG conversion efficiency than AGS. Moreover, the high-yield, congruent-melting behavior, along with relatively low melting/crystallizing points of all the compounds studied make them feasible to grow large single crystals needed for practical applications using the well-known Bridgman method. All these findings suggest that the title compounds are potentially good candidates for IR-NLO materials and efforts to grow bulk crystals are in progress. Moreover, the current studies also show that the alkali metal halide salts in the salt-inclusion chalcogenides may serve as a structure directing agent during the formation of the NCS compounds, which provides a new opportunity to design new structure-directing functional materials.

Acknowledgements

We gratefully acknowledge financial support from Strategic Priority Research Program of the CAS (XDB20000000), the NSF of China (91222204, 21403231, and 21303203) and the NSF of Fujian Province (2014J05025, 2013J05034).

Notes and references

1 (*a*) V. A. Serebryakov, E. V. Boiko, N. N. Petrishchev and A. V. Yan, *J. Opt. Technol.*, 2010, **77**, 6–17; (*b*) W. Chen, G. Mouret, D. Boucher and F. K. Tittel, *Appl. Phys. B: Lasers Opt.*, 2001, **72**, 873–876; (*c*) C. T. Chen and G. Z. Liu, *Annu. Rev. Mater. Sci.*, 1986, **16**, 203–243; (*d*) P. J. Pauzauskie and P. Yang, *Mater. Today*, 2006, **9**, 36–45; (*e*) P. F. Bordui and M. M. Fejer, *Annu. Rev. Mater. Sci.*, 1993, **23**, 321–379.
2 J. F. Ward and P. A. Franken, *Phys. Rev.*, 1964, **133**, A183–A190.
3 K. Kato, *IEEE J. Quantum Electron.*, 1991, **27**, 1137–1140.
4 C. T. Chen, B. C. Wu, A. D. Jiang and G. M. You, *Sci. Sin., Ser. B*, 1985, **28**, 235–243.
5 C. T. Chen, Y. C. Wu, A. D. Jiang, B. Wu, G. M. You, R. K. Li and S. J. Lin, *J. Opt. Soc. Am. B*, 1989, **6**, 616–621.
6 A. Harasaki and K. J. Kato, *Appl. Phys.*, 1997, **36**, 700–703.
7 G. C. Catella, L. R. Shiozawa, J. R. Hietanen, R. C. Eckardt, R. K. Route, R. S. Feigelson, D. G. Cooper and C. L. Marquardt, *Appl. Opt.*, 1993, **32**, 3948–3951.
8 G. D. Boyd, E. Buehler and F. G. Storz, *Appl. Phys. Lett.*, 1971, **18**, 301–304.
9 L. Kang, M. L. Zhou, J. Y. Yao, Z. S. Lin, Y. C. Wu and C. T. Chen, *J. Am. Chem. Soc.*, 2015, **137**, 13049–13059.
10 L. Isaenko, A. Yelisseyev, S. Lobanov, P. Krinitsin, V. Petrov and J. J. Zondy, *J. Non-Cryst. Solids*, 2006, **352**, 2439–2443.

11 L. Isaenko, I. Vasilyeva, A. Yelisseyev, S. Lobanov, V. Malakhov, L. Dovlitova, J. J. Zondy and I. Kavun, *J. Cryst. Growth*, 2000, **218**, 313–322.
12 Y. Kim, I. S. Seo, S. W. Martin, J. Baek, P. S. Halasyamani, N. Arumugam and H. Steinfink, *Chem. Mater.*, 2008, **20**, 6048–6052.
13 X. S. Lin, G. Zhang and N. ye, *Cryst. Growth Des.*, 2009, **9**, 1186–1189.
14 M. Zhang, S. Pan, Z. Yang, Y. Wang, X. Su, Y. Yang, Z. Huang, S. Han and K. R. Poeppelmeier, *J. Mater. Chem. C*, 2013, **1**, 4740–4745.
15 G. Zhang, J. G. Qin, T. Liu, Y. J. Li, Y. C. Wu and C. T. Chen, *Appl. Phys. Lett.*, 2009, **95**, 261104.
16 G. Zhang, Y. J. Li, K. Jiang, H. Y. Zeng, T. Liu, X. G. Chen, J. G. Qin, Z. S. Lin, P. Z. Fu, Y. C. Wu and C. T. Chen, *J. Am. Chem. Soc.*, 2012, **134**, 14818–14822.
17 (*a*) W. L. Queen, J. P. West, S.-J. Hwu, D. G. VanDerveer, M. C. Zarzyczny and R. A. Pavlick, *Angew. Chem., Int. Ed.*, 2008, **47**, 3791–3794; (*b*) S.-J. Hwu, M. Ulutagay-Kartin, J. A. Clayhold, R. Mackay, T. A. Wardojo, C. J. O'Connor and M. Krawiec, *J. Am. Chem. Soc.*, 2002, **124**, 12404–12405.
18 X. Li, L. Kang, C. Li, Z. Lin, J. Yao and Y. Wu, *J. Mater. Chem. C*, 2015, **3**, 3060–3067.
19 Z. Z. Luo, C. S. Lin, H. H. Cui, W. L. Zhang, H. Zhang, Z. Z. He and W. D. Cheng, *Chem. Mater.*, 2014, **26**, 2743–2749.
20 S. M. Kuo, Y. M. Chang, M. Chung, J. I. Jang, B. H. Her, S. H. Yang, J. B. Ketterson, M. G. Kanatzidis and K. F. Hsu, *Chem. Mater.*, 2013, **25**, 2427–2433.
21 S. Banerjee, J. M. Szarko, B. D. Yuhas, C. D. Malliakas, L. X. Chen and M. G. Kanatzidis, *J. Am. Chem. Soc.*, 2010, **132**, 5348–5350.
22 Y. Wu and W. Bensch, *Inorg. Chem.*, 2008, **17**, 7523–7534.
23 B. J. Chen, S. F. Zhu, B. J. Zhao, J. J. Zhang, Y. Huang, M. Li, J. Liu, B. Tan, R. L. Wang and Z. Y. He, *J. Cryst. Growth*, 2006, **292**, 490–493.
24 L. Isaenko, I. Vasilyeva, A. Merkulov, A. Yelisseyev and S. Lobanov, *J. Cryst. Growth*, 2005, **275**, 217–223.
25 J. A. Brant, D. J. Clark, Y. S. Kim, J. Y. Jang, J. H. Zhang and J. A. Aitken, *Chem. Mater.*, 2014, **26**, 3045–3048.
26 G. C. Bhar and R. C. Smith, *Phys. Status Solidi A*, 1972, **13**, 157–168.
27 C. R. Evenson IV and P. K. Dorhout, *Inorg. Chem.*, 2001, **40**, 2884–2891.
28 S. K. Kurtz and T. T. Perry, *J. Appl. Phys.*, 1968, **39**, 3798–3813.
29 G. C. Bhar, *Jpn. J. Appl. Phys.*, 1993, **32**, 653–659.
30 (*a*) M.-J. Zhang, X.-M. Jiang, L.-J. Zhou and G.-C. Guo, *J. Mater. Chem. C*, 2013, **1**, 4754–4760; (*b*) M.-J. Zhang, B.-X. Li, B.-W. Liu, Y.-H. Fan, X.-G. Li, H.-Y. Zeng and G.-C. Guo, *Dalton Trans.*, 2013, **42**, 14223–14229; (*c*) Q. Wu, X. G. Meng, C. Zhong, X. G. Chen and J. G. Qin, *J. Am. Chem. Soc.*, 2014, **136**, 5683–5686; (*d*) J. A. Brant, D. J. Clark, Y. S. Kim, J. I. Jang, A. Weiland and J. A. Aitken, *Inorg. Chem.*, 2015, **54**, 2809–2819.
31 Y. Y. Li, P. F. Liu, L. Hu, L. Chen, H. Lin, L. J. Zhou and L. M. Wu, *Adv. Opt. Mater.*, 2015, **7**, 957–966.
32 H. Zhang, M. Zhang, S. Pan, X. Dong, Z. Yang, X. Hou, Z. Wang, K. B. Chang and K. R. Poeppelmeier, *J. Am. Chem. Soc.*, 2015, **137**, 8360–8363.
33 K. A. Rosmus, J. A. Brant, S. D. Wisneski, D. J. Clark, Y. S. Kim, J. I. Jang, C. D. Brunetta, J.-H. Zhang, M. N. Srnec and J. A. Aitken, *Inorg. Chem.*, 2014, **53**, 7809–7811.
34 J. I. Jang, D. J. Clark, J. A. Brant, J. A. Aitken and Y. S. Kim, *Opt. Lett.*, 2014, **39**, 4579–4582.
35 K. Wu, Z. Yang and S. Pan, *Angew. Chem., Int. Ed.*, 2016, **53**, 6713–6715.
36 K. Wu, Z. Yang and S. Pan, *Chem. Mater.*, 2016, **28**, 2795–2801.
37 Z.-Z. Luo, C.-S. Lin, W.-L. Zhang, H. Zhang, Z.-Z. He and W.-D. Cheng, *Chem. Mater.*, 2014, **26**, 1093–1099.
38 B.-W. Liu, H.-Y. Zeng, M.-J. Zhang, Y.-H. Fan, G.-C. Guo, J.-S. Huang and Z.-C. Dong, *Inorg. Chem.*, 2015, **54**, 976–981.
39 J. A. Brant, D. J. Clark, Y. S. Kim, J. I. Jang, A. Weiland and J. A. Aitken, *Inorg. Chem.*, 2015, **54**, 2809–2819.